UDC 551.501.75:551.558.2:551.511.2:551.509.312

On the Estimation of Kinematic Parameters in the Atmosphere From Radiosonde Wind Data

HARRISON CHIEN and PHILLIP J. SMITH [1]—*Department of Geosciences, Purdue University, Lafayette, Ind.*

ABSTRACT—A technique is proposed for computing horizontal velocity divergence and the vertical component of vorticity from radiosonde wind data. Utilizing a quadratic Taylor's series representation of the horizontal wind field, one can consider nonlinear variations in the wind directly in estimates of the first-order derivatives of the wind components. These nonlinear variations are found to be significant in a number of cases. Vertical motions computed by the kinematic method and horizontal divergence are modified by an adjustment scheme. Comparison of these results with those derived from computations from a linear Taylor's series representation of the wind suggests that the quadratic model is superior to the linear. Synoptic analyses of vorticity, divergence, and vertical motions over the United States at 0000 and 1200 GMT on Apr. 13, 1964, reveal good agreement with the circulation patterns and associated weather.

1. INTRODUCTION

Because of inadequate numerical and/or physical modeling and erroneous or insufficient data, reliable computations of derived kinematic parameters using radiosonde wind data are difficult to obtain. This is particularly true of horizontal wind divergence and the resulting vertical motion. Relatively simple and convenient methods for computing horizontal divergence have been described by Bellamy (1949), Panofsky (1951), and Graham (1953). Although their computational techniques differ, these methods share a common assumption; namely, that the wind field varies linearly between gridpoints or observation points.

After the advent of electronic computers, the magnitude of the calculations was no longer an obstacle in efforts to estimate divergence and vorticity. Endlich and Clark (1963) calculated many dynamic as well as thermodynamic variables, including three-dimensional vorticity, divergence, and vertical motion. Divergence and vorticity were computed at three stations that form a triangle. Their procedure is to first estimate a wind value, $\overline{V}_0$, at the centroid of the triangle. Assuming a linear variation in the wind field over the triangle, they then represent the wind at each vertex ($i=1,2,3$) by a linear, two-dimensional Taylor's series. Subtracting equations for point 1 from 2 and 1 from 3, they derive two simultaneous equations that can be solved for the vector derivatives at the triangle centroid. These derivatives are then used to provide estimates of vorticity and divergence. As a basis for numerical forecasting, where short waves are smoothed or suppressed, their results are encouraging. However, they note that the assumption of linear variations of the wind field, though defensible on the grounds of simplicity and reasonable accuracy in their studies, certainly cannot be applied across the jet streams, over mountain areas, or in convective regions where nonlinear variations are apparent.

The values of quantities such as divergence computed from simultaneous rawinsonde observations by use of the triangle routine will contain noise due to erroneous data and the assumption of linearity. As pointed out by Endlich and Clark (1963), one means of reducing noise would be to base the computations on data from more than three stations. To consider nonlinear variations in the wind field, one could add terms containing the second-order derivatives of the wind field to the Taylor's expansion by adding data from additional stations. Endlich and Clark felt that this refinement would provide improved results. The importance of incorporating nonlinearities in the wind field in horizontal divergence calculations has also been noted by Fankhauser (1969) and Schmidt and Johnson (1972).

The research reported in this paper is in accord with the suggestion of Endlich and Clark (1963). It also parallels in some ways the work of Schmidt and Johnson, although the present calculations do not include their polynomial filtering technique.

2. COMPUTATION OF KINEMATIC PARAMETERS

Consider six stations observing wind data, with station 0 located inside the pentagon formed by stations 1 through 5. An approximate expression for the wind components at stations 1 through 5 can be obtained from a truncated, two-dimensional Taylor's series expanded about station 0.

[1] On leave of absence to The Advanced Study Program at the National Center for Atmospheric Research, Boulder, Colo.

Thus, the component equations can be written as

$$u_i=u_0+\left(\frac{\partial u}{\partial x}\right)_0(x_i-x_0)+\left(\frac{\partial u}{\partial y}\right)_0(y_i-y_0)+\frac{1}{2!}\left[\left(\frac{\partial^2 u}{\partial x^2}\right)_0(x_i-x_0)^2\right. \tag{1}$$

$$\left.+2\left(\frac{\partial^2 u}{\partial x\partial y}\right)_0(x_i-x_0)(y_i-y_0)+\left(\frac{\partial^2 u}{\partial y^2}\right)_0(y_i-y_0)^2\right] \qquad i=1\text{–}5$$

and

$$v_i=v_0+\left(\frac{\partial v}{\partial x}\right)_0(x_i-x_0)+\left(\frac{\partial v}{\partial y}\right)_0(y_i-y_0)+\frac{1}{2!}\left[\left(\frac{\partial^2 v}{\partial x^2}\right)_0(x_i-x_0)^2\right. \tag{2}$$

$$\left.+2\left(\frac{\partial^2 v}{\partial x\partial y}\right)_0(x_i-x_0)(y_i-y_0)+\left(\frac{\partial^2 v}{\partial y^2}\right)_0(y_i-y_0)^2\right] \qquad i=1\text{–}5$$

where u and v are the east–west and north–south wind components and x and y are the east–west and north–south spatial coordinates on a spherical earth. For the u_i or v_i family of simultaneous equations, the unknowns are the five derivative terms at the center station 0, since all u_is and v_is and u_0 and v_0 are observed and all (x_i-x_0) and (y_i-y_0) are known distances.

After solving the above equations, one can compute the divergence and vorticity values for station 0 as

$$\nabla_H\cdot\mathbf{V}=\left(\frac{\partial u}{\partial x}\right)_0+\left(\frac{\partial v}{\partial y}\right)_0-\frac{v_0\tan\phi_0}{r} \tag{3}$$

and

$$\zeta=\left(\frac{\partial v}{\partial x}\right)_0-\left(\frac{\partial u}{\partial y}\right)_0+\frac{u_0\tan\phi_0}{r} \tag{4}$$

where ϕ_0 is the latitude of the center station and r is the earth's radius. The same procedure can be applied at each station, regarding it as the center station with its own five surrounding stations. The added terms

$$-\frac{v_0\tan\phi_0}{r}$$

and

$$\frac{u_0\tan\phi_0}{r}$$

in the divergence and vorticity computations are required to account for a spherical curvilinear coordinate system (Haltiner and Martin 1957). These divergence and vorticity values, though still expressed in terms of the simple first-order derivatives of the wind field, include through eq (1) and (2) the influence of the second-order derivatives, which represent nonlinear variations of the wind field. Theoretically, the values of even higher order derivatives of the wind field could be obtained by choosing more stations around station 0. However, a larger cluster of surrounding stations is difficult to achieve without greatly expanding the local region, which tends to negate any advantages gained from the addition of higher order nonlinearities.

The data used in the study were standard radiosonde wind observations for North America,[2] with computations performed at the array of 70 stations enclosed by the heavy black line in figure 1. The remaining stations in figure 1 were required for computations at the boundary of the region. In the vertical, data were provided at the surface and in 50-mb increments from the first standard pressure level above the surface. The data used in this study extended to 200 mb for the period Apr. 10–16, 1964 (0000 and 1200 GMT), an excellent example of midlatitude cyclone development. Procedures adopted to interpolate missing wind data are described in the appendix.

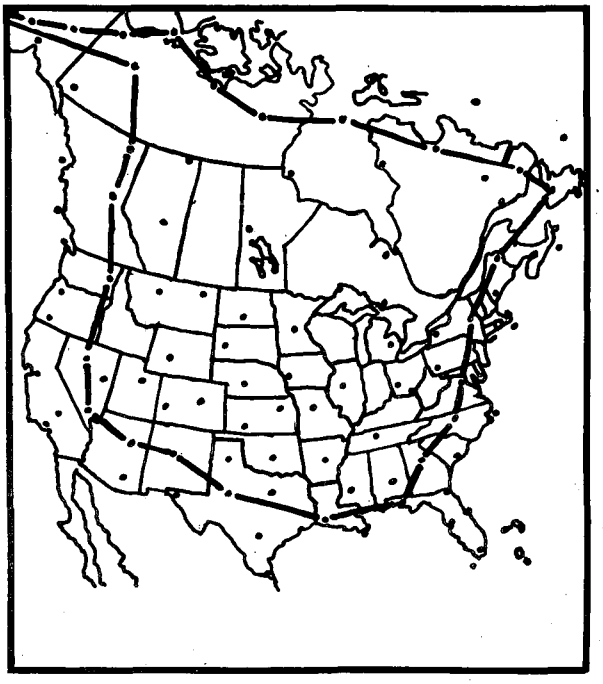

FIGURE 1.—Radiosonde stations utilized for derivative computations (enclosed by heavy black line) and as additional boundary points.

The influences of second-order derivatives of the wind field are examined by comparing the order of magnitude of the individual derivative terms computed at each station multiplied by the corresponding mean distance from the center station to its five surrounding stations in the original array. These values can then be regarded as the relative influences of the individual derivatives on the total wind field in the Taylor's expansion. The results in table 1 indicate that in many cases the second-order terms are of equal or greater order of magnitude than the corresponding first-order terms, demonstrating the presence of nonlinear variations of the wind field. The nonlinearities are somewhat more prominent at 850 mb than at 500 and 300 mb, perhaps reflecting the dominant role of the major low-level cyclone from the 12th to the 16th of the month. These nonlinear terms will not always influence the first-order derivatives significantly because of differences in signs, but, in view of Schmidt and Johnson's (1972) conclusions, nonlinearities are likely to be important for a number of stations.

Although divergence and vorticity values obtained in this fashion are objective and are presumably based on a more realistic computational model, there are still com-

[2] Provided by National Climatic Center, NOAA.

TABLE 1.—*Percent of cases in which quadratic terms exhibited equal or greater order of magnitude than the corresponding linear terms; 0000 GMT, Apr. 10–1200 GMT, Apr. 16, 1964*

Level	Linear Term	$\frac{\partial^2 u}{\partial x^2}\frac{\overline{\Delta x}^2}{2}$	$\frac{\partial^2 u}{\partial x \partial y}\overline{\Delta x}\,\overline{\Delta y}$	$\frac{\partial^2 u}{\partial y^2}\frac{\overline{\Delta y}^2}{2}$
(mb)				
850	$\frac{\partial u}{\partial x}\overline{\Delta x}$	25	37	
500		25	37	
300		20	34	
850	$\frac{\partial u}{\partial y}\overline{\Delta y}$		27	29
500			27	27
300			25	23
		$\frac{\partial^2 v}{\partial x^2}\frac{\overline{\Delta x}^2}{2}$	$\frac{\partial^2 v}{\partial x \partial y}\overline{\Delta x}\,\overline{\Delta y}$	$\frac{\partial^2 v}{\partial y^2}\frac{\overline{\Delta y}^2}{2}$
850	$\frac{\partial v}{\partial x}\overline{\Delta x}$	24	31	
500		20	28	
300		17	26	
850	$\frac{\partial v}{\partial y}\overline{\Delta y}$		36	31
500			28	27
300			28	25

putational limitations involved in the method. These may be divided into two categories. The first includes observational error and scarcity of data in time and space; the second is related to the particular assumptions or operations involved in the computational model. From Duvedal (1962), it may be concluded that errors in both wind direction and speed due to observational methods average about 10 percent. Duvedal also pointed out that, in the extreme case when one tries to compute high-level wind with small elevation angle and large speed, the error involved in neglecting the curvature of the surface of the earth alone could cause a maximum of 21-percent error in computing wind speed. In general, however, 10-percent error is considered standard. The influence of erroneous wind data on computed divergence has been noted by Landers (1955) and Thompson (1961). Landers indicated that a 5-percent error in wind speed at one end of the finite-difference distance of differentiation and a true wind speed at the other end caused errors varying from 30 to 50 percent depending on the magnitude of divergence. Thompson pointed out that a 10-percent error in the observed winds could lead to 100-percent errors in divergence.

Before examining the divergence errors encountered in this study, one must consider the vertical motion estimates. Techniques for computing vertical motion have been classsified by Miller and Panofsky (1958) as precipitation, adiabatic, vorticity, numerical, and kinematic methods. In addition, Danielsen (1966) has described the use of isentropic trajectories for these computations. Of these techniques, the adiabatic (Panofsky 1951), numerical (Elsaesser 1960, Cressman 1963, O'Neill 1966, Krishnamurti 1968*a*, 1968*b*), and kinematic (Lateef 1967, Kreitzberg 1968, Fankhauser 1969, O'Brien 1970, Smith 1971, Kung 1972) methods have found the widest application. Advantages and disadvantages of these methods have been noted by Panofsky, O'Neill, O'Brien, and Smith.

To further test the quality of the divergence estimates in this study, we used the kinematic method to compute vertical motion. The continuity equation in pressure coordinates can be written as

$$\frac{\partial u}{\partial x}+\frac{\partial v}{\partial y}+\frac{\partial \omega}{\partial p}=0 \tag{5}$$

where the vertical motion $\omega=dp/dt$. Integrating with respect to p from a low level, p_i, to a higher level, p_{i+1}, we can express vertical motion at the higher level, p_{i+1}, as

$$\omega_{p_{i+1}}=\omega_{p_i}-\int_{p_i}^{p_{i+1}}(\nabla_H\cdot\mathbf{V})dp. \tag{6}$$

Assuming that ω is known at the lower boundary, we can compute $\omega_{p_{i+1}}$ at each successively higher level. The principal advantage of this method rests in its simplicity. In addition, the only physical assumption made is hydrostatic balance, realistic for large-scale atmospheric motions. It would undoubtedly be preferred over other methods were it not for the serious problem encountered in the vertical integration of horizontal divergence.

Because of the basic dependence of the kinematic method on the divergence field, it cannot be applied using a simplified nondivergent representation of the wind. Instead, actual horizontal wind data must be utilized. As noted earlier, systematic errors can lead to biased divergence estimates, the magnitude of which depend on the computing technique used. These biased errors tend to accumulate upon integration, often producing unrealistically large values of vertical motions in the upper troposphere. To minimize cumulative bias errors, Lateef (1967), Kreitzberg (1968), Fankhauser (1969), and Smith (1971) utilized empirical adjustment techniques. Recently, Kung (1972) proposed an optimization method in which kinematic vertical motion estimates are made using several computational models, and the best estimate is chosen as that profile which most nearly converges to zero at the upper levels.

A comprehensive analysis of adjustment techniques has been made by O'Brien (1970). The current study utilizes the technique proposed by O'Brien in which the error in the mean divergence for each layer is assumed to be a linear function of the net ω error determined at the top of an atmospheric column. This technique is based on the reasonable assumption that the divergence errors arising from erroneous data become more pronounced at higher levels where wind data are least reliable. As applied by Fankhauser, O'Brien's adjustment

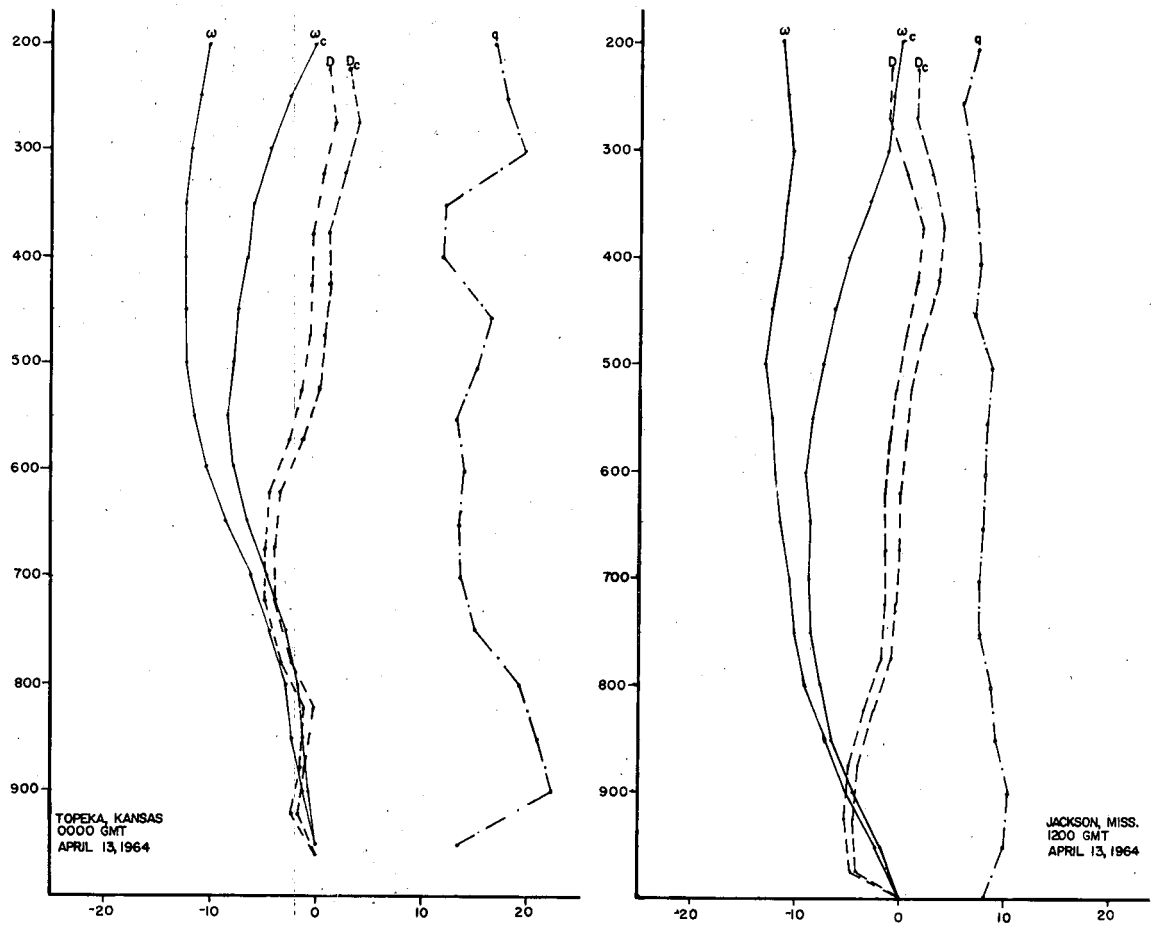

FIGURE 2.—Vertical profiles of original and adjusted divergence, D and D_c ($10^{-5}s^{-1}$), vertical motion, ω and ω_c (μbar/s), and absolute vorticity, Q ($10^{-5}s^{-1}$).

equations become

$$\overline{(\nabla\cdot\mathbf{V})}'_k=\overline{(\nabla\cdot\mathbf{V})}_k-\frac{k}{M\Delta p}(\omega_K-\omega_T) \tag{7}$$

and

$$\omega'_k=\omega_k-(\omega_K-\omega_T)\left[\frac{k(k+1)}{K(K+1)}\right] \tag{8}$$

where the primed quantities represent the adjusted values, k is the specific level where the adjustment is desired, K is the total number of levels involved, M is $\frac{1}{2}K(K+1)$, ω_K is the computed vertical motion at the top level, ω_T is the correct value of vertical motion at the top level (assumed to be 0), Δp is the pressure interval that evenly divides each data level, and the overbar indicates a vertical average over the interval Δp.

The maximum divergence adjustment occurs high in the atmosphere, while near the ground the correction is essentially zero. Similarly, the weighted adjustment for ω, which is almost quadratic, is essentially zero in the lower part of the atmosphere and maximum at upper levels.

Vertical profiles of the original divergence, D, versus adjusted divergence, D_c, and original vertical motion, ω, versus adjusted vertical motion, ω_c, for Topeka, Kans., at 0000 GMT and Jackson, Miss., at 1200 GMT on Apr. 13, 1964, are shown in figure 2. The dashed lines represent original and adjusted values of divergence, and the solid lines represent original and adjusted values of

TABLE 2.—*Average absolute adjusted divergence,* $|\tilde{D}_c|$, *quadratic divergence error,* $|\tilde{E}_q|$, *percentage error,* $\tilde{P}E$, *linear divergence error,* $|\tilde{E}_l|$, *and model error,* $\tilde{E}_m$, *for Apr. 10–Apr. 16, 1964*

Pressure (mb)	$\lvert\tilde{D}_c\rvert$ ($10^{-5}s^{-1}$)	$\lvert\tilde{E}_q\rvert$ ($10^{-5}s^{-1}$)	*PE*	$\lvert\tilde{E}_l\rvert$ ($10^{-5}s^{-1}$)	$\tilde{E}_m$ ($10^{-5}s^{-1}$)
950	0.25	0.02	8	0.02	−0.10
900	.52	.10	19	.11	.12
850	.63	.15	24	.20	.47
800	.68	.21	31	.30	.64
750	.64	.26	41	.41	.87
700	.64	.32	50	.52	.99
650	.59	.36	61	.62	.94
600	.59	.44	75	.72	.95
550	.58	.48	83	.82	.95
500	.57	.54	95	.92	.86
450	.61	.59	97	1.02	.85
400	.68	.66	97	1.12	.94
350	.81	.70	86	1.22	1.04
300	.86	.76	88	1.32	1.18
250	.89	.81	91	1.42	1.22
200	.93	.89	96	1.52	1.25

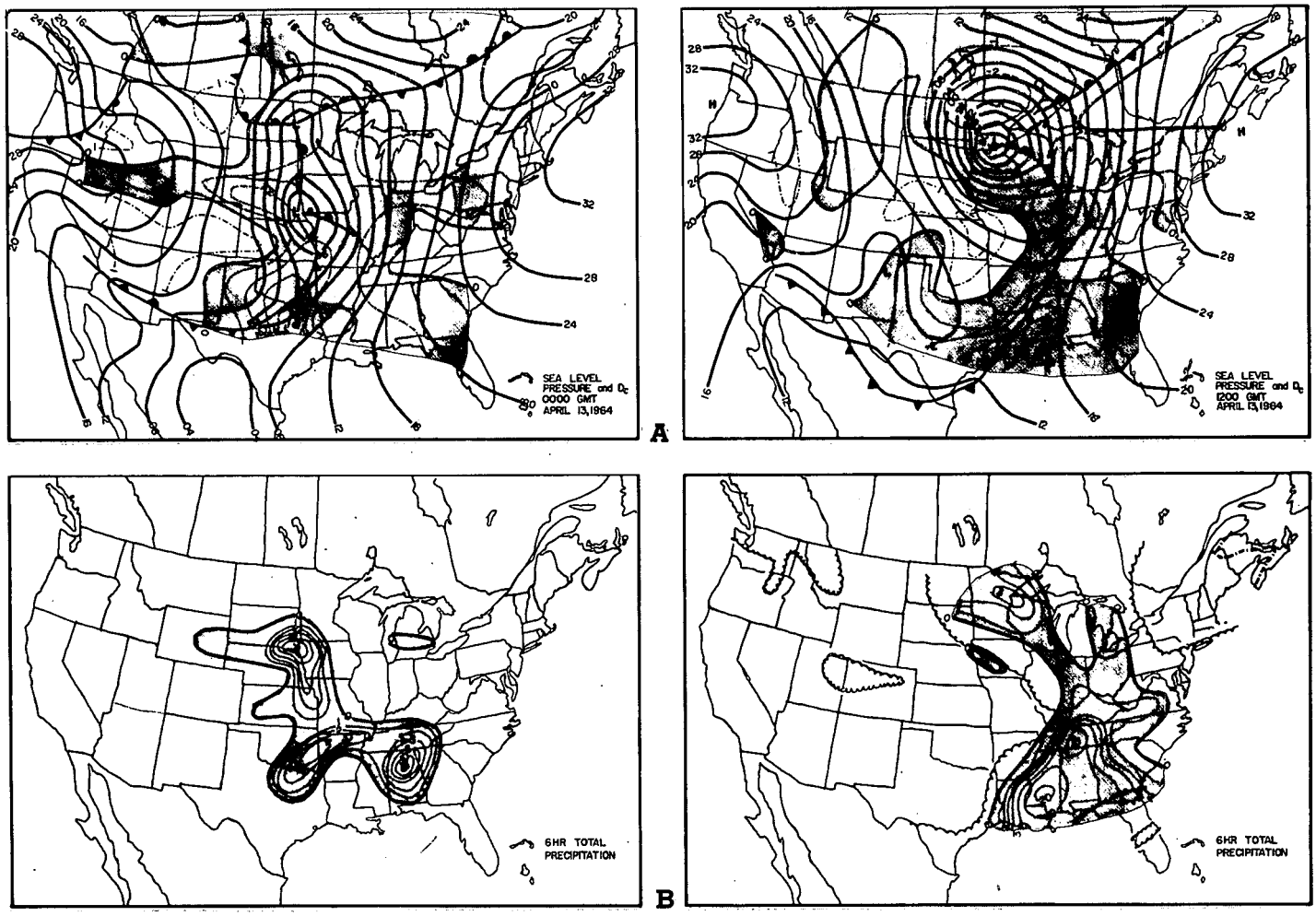

FIGURE 3.—(A) sea-level pressure (solid lines, mb) and second standard level divergence (dashed lines, $10^{-5}s^{-1}$). Convergence areas (negative values) are shaded. (B) total precipitation (0.1 in.) from 3 hr before to 3 hr after upper air map times. Areas of 7/8 to 8/8 cloud cover are scalloped at 1200 GMT.

vertical motion. These two cases were chosen because they represent extreme examples of errors in ω and D. Maximum adjustment at higher levels is readily seen. Also, adjustments of D are obviously less severe than those of ω. Since $\omega_T=0$ is assumed to be the "correct" value at 200 mb, any deviations in ω_c from ω and D_c from D may be interpreted as "errors" induced by bias in the original data. A summary of error estimates is given in table 2. The first three columns show the average absolute value of D_c, assumed to be the correct value of divergence; the average absolute error, $|\tilde{E}_q|$, as derived from the quadratic model calculations of D; and the average percentage error, $PE=|\tilde{E}_q|/|\tilde{D}_c|$, for each pressure level. A second set of divergence estimates were computed from a linear Taylor's series expansion adopting the procedures of Endlich and Clark (1963). Following the same adjustment scheme, corrected divergence estimates, D_l, and corresponding bias errors resulting from the linear model were calculated. The absolute average linear model errors are given in table 2 as $|\tilde{E}_l|$. Finally, the difference between $|\tilde{D}_c|$ and $|\tilde{D}_l|$ is utilized as a measure of the error that remains in D_l as a result of not considering quadratic variations in the wind field. These are referred to as model errors and are represented as $\tilde{E}_m=|\tilde{D}_l|-|\tilde{D}_c|$.

As required by the adjustment technique, the absolute errors increase with decreasing pressure, reflecting the diminishing reliability of wind data at higher elevations. It is apparent upon comparing $|\tilde{E}_q|$ with $|\tilde{E}_l|$ that bias errors induced in the linear model substantially exceed those given by the quadratic model except in the lowest layers. The similarity of the two models in the lowest layers is also seen in $\tilde{E}_m$. Apparently, even though table 1 shows significant contribution from nonliner terms at 850 mb, the magnitude of all of the derivative terms is so small near the ground that the addition of quadratic effects has relatively little influence on the divergence computations. From 850 mb to 200 mb, the results suggest that modeling errors may exceed those due to biased wind data. This is analogous to Fankhauser's (1968) conclusion for a mesoscale data network, that failure to produce realistic vertical motions as determined by horizontal divergence at high levels is due mainly to the cumulative effect of unresolved nonlinearities in the wind analyses, rather than from shortcomings in the measurement of the winds. The precentage errors, PE,

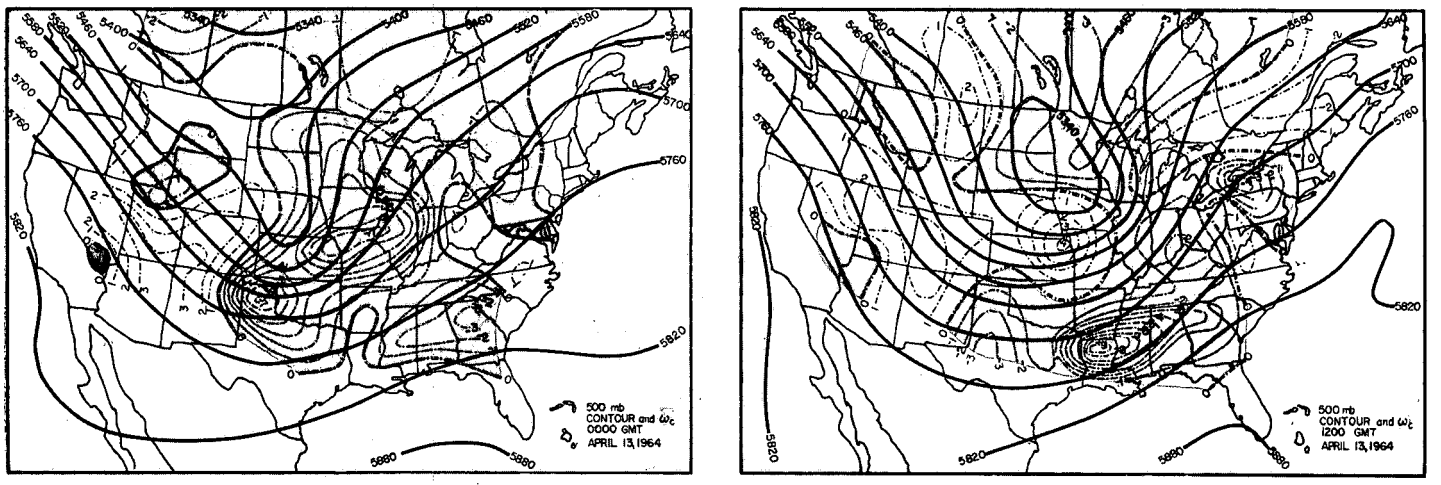

FIGURE 4.—The 500-mb contours (solid lines, m) with adjusted vertical motions, ω_c, (dash-dot lines, μbar/s). Upward motion areas (negative values) are shaded.

accounted for by the adjustment scheme, which become large in the higher levels, are nevertheless in accord with those expected from wind data errors (Landers 1955, Thompson 1961).

To this point, little has been said about the vorticity computations. It is well known that vorticity calculations are consistently more reliable than divergence calculations (e.g., Haltiner and Martin 1957) and thus do not require the application of adjustment techniques. Included in figure 2 are the vertical profiles of absolute vorticity for the two stations noted earlier. As may be seen by examining the figures to follow, Topeka, Kans., is in a region of strong cyclonic development with an upper air trough to the west and, hence, exhibits strong absolute vorticity. Jackson, Miss., on the other hand, is well south of the surface cyclone, with nearly linear low-level flow and weak anticyclonic shear aloft, both of which correspond well with the weak absolute vorticity profile.

3. SYNOPTIC ANALYSIS

Based on the results described in the previous section, the synoptic analyses utilize adjusted horizontal divergence and vertical motion and original absolute vorticity estimates, all based on the quadratic Taylor's series model. Further, to conserve space, we have limited the discussion to two map times, 0000 and 1200 GMT on Apr. 13, 1964. The basic synoptic situation for this period is depicted by the surface, 500-mb, and 300-mb charts given in figures 3–5. Isobar and contour analyses are taken directly from National Meteorological Center (NMC) analyses.[3] Precipitation data were read from the Daily Precipitation Tables,[3] while total cloud cover was derived from the 1200 GMT synoptic data in the Northern Hemisphere Data Tabulation.[3]

On the 0000 GMT surface map (fig. 3), the major features are a deepening Low over southeastern Nebraska, an associated advancing cold front, and a following high-pressure ridge. Figure 3 also shows the pattern of total precipitation for the period 3 hr before to 3 hr after each map time. At 0000 GMT, three precipitation maxima occur, one of 0.6 in. associated with the Low, another of 0.4 in. in advance of the cold front in the southern States, and a third of 1.6 in. over central Alabama. Prominent at 500 mb (fig. 4) during this map time is a trough extending from North Dakota south through western Texas. Much of the central United States is dominated by cyclonic flow, while the region north and east of Minnesota and the Great Lakes experienced anticyclonic flow. Note the very sharp curvature in the trough in northern Kansas. Also prominent in the upper air flow is the 300-mb wind maximum (fig. 5) west of the trough.

By 1200 GMT, the surface Low has deepened from a sea-level pressure of 992 to 976 mb. The first two precipitation maxima noted for 0000 GMT persist, but the maximum associated with the Low has decreased to only 0.40 in., while that ahead of the cold front has increased to 2.0 in. The 500-mb wave has deepened, with a closed Low appearing. The area of cyclonic flow has expanded, but the sharp curvature noted at 0000 GMT has disappeared. The 300-mb wind maximum has moved to the southern and eastern portions of the wave.

Absolute Vorticity

Figure 6 shows the vertical component of absolute vorticity at 500 mb for 0000 and 1200 GMT on April 13. Figure 6A represents the calculations of this study, while figure 6B shows reproductions of NMC analyses. The solid lines represent isopleths of absolute vorticity in units 10^{-5} s^{-1}. At 0000 GMT, the 500-mb flow pattern suggests that a vorticity maximum should be expected in the vicinity of the Low center and the major trough because of the very strong cyclonic curvature. This feature is well reflected both in vorticity computations of this study and those of NMC. Notice that the trough shows good correlation with the maximum vorticity line. A computed maximum of 18×10^{-5} s^{-1} occurs in central Kansas in accord with the NMC maximum of the same magnitude at the Kansas-Nebraska border. The general vorticity distribution near this maximum shows good agreement between this study and the NMC output.

[3] Provided by National Climatic Center, NOAA.

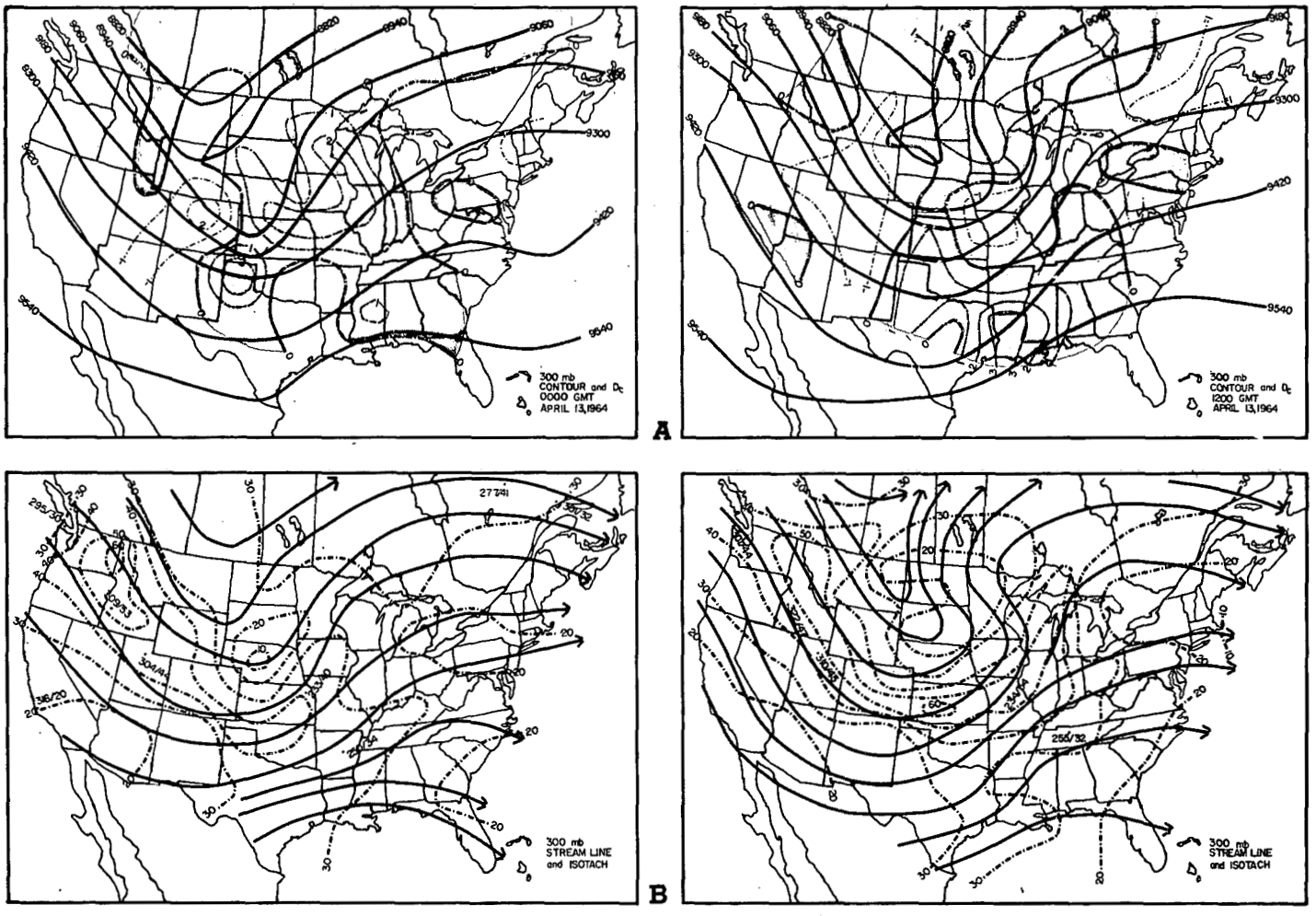

FIGURE 5.—(A) 300-mb contours (solid lines, m) and divergence (dashed lines, $10^{-5}s^{-1}$). Divergence areas (positive values) are shaded. (B) 300-mb streamlines (solid lines) and isotachs (dashed lines, m/s). Interpolated winds at missing data stations are included.

Another computed maximum of 12×10^{-5} s^{-1} can be associated with the minor trough over Lake Ontario, Ohio, and West Virginia. The corresponding NMC result shows a maximum of 10×10^{-5} s^{-1} over the same area. Neither result catches the minimum that might be expected with the ridge extending from Wisconsin to Michigan, although some lower values are found in that general area.

At 1200 GMT, the major trough extends from eastern Iowa through western Kansas, Oklahoma, and western Texas. Again, this area agrees well with the location of the computed vorticity maximum. A computed maximum center of 18×10^{-5} s^{-1} covers most of the eastern part of North and South Dakota, Nebraska, and the western part of Wisconsin and Iowa. The NMC result shows a larger maximum of 20×10^{-5} s^{-1} in central Iowa; however, the general areas covered by the maxima coincide closely. This maximum area also extends eastward to central Michigan, associated with the secondary trough at 500 mb in that region.

The minimum of 8×10^{-5} s^{-1} to the east of the maximum center matches the ridge at 500 mb in that region in both results. The excellent comparison of the NMC estimates, which assume linear variations in their stream function representation of the wind, with the results of the nonlinear model is perhaps surprising. However, table 1 suggests that one might expect linear variations to dominate over 70 to 80 percent of the gridpoints. Thus, the authors' maps should compare well with NMC products if a consistent representation of the voriticity field is being presented.

Although the total area influenced by the larger vorticities (e.g., 14 and 16 isopleths) and, hence, the total vorticity associated with the 500-mb wave has increased with the wave's development, the computations of this study show no corresponding increase in the maximum. The authors feel that the maximum at 0000 GMT has been greatly influenced by the strong curvature in northern Kansas. By 1200 GMT, this strong curvature has disappeared but has been replaced by stronger cyclonic shear, suggesting that little change in the absolute vorticity maximum might be expected.

Horizontal Divergence

Divergence estimates are shown for both lower (second standard level) and upper (300 mb) levels in figures 3 and 5. The dashed lines represent divergence (+) and

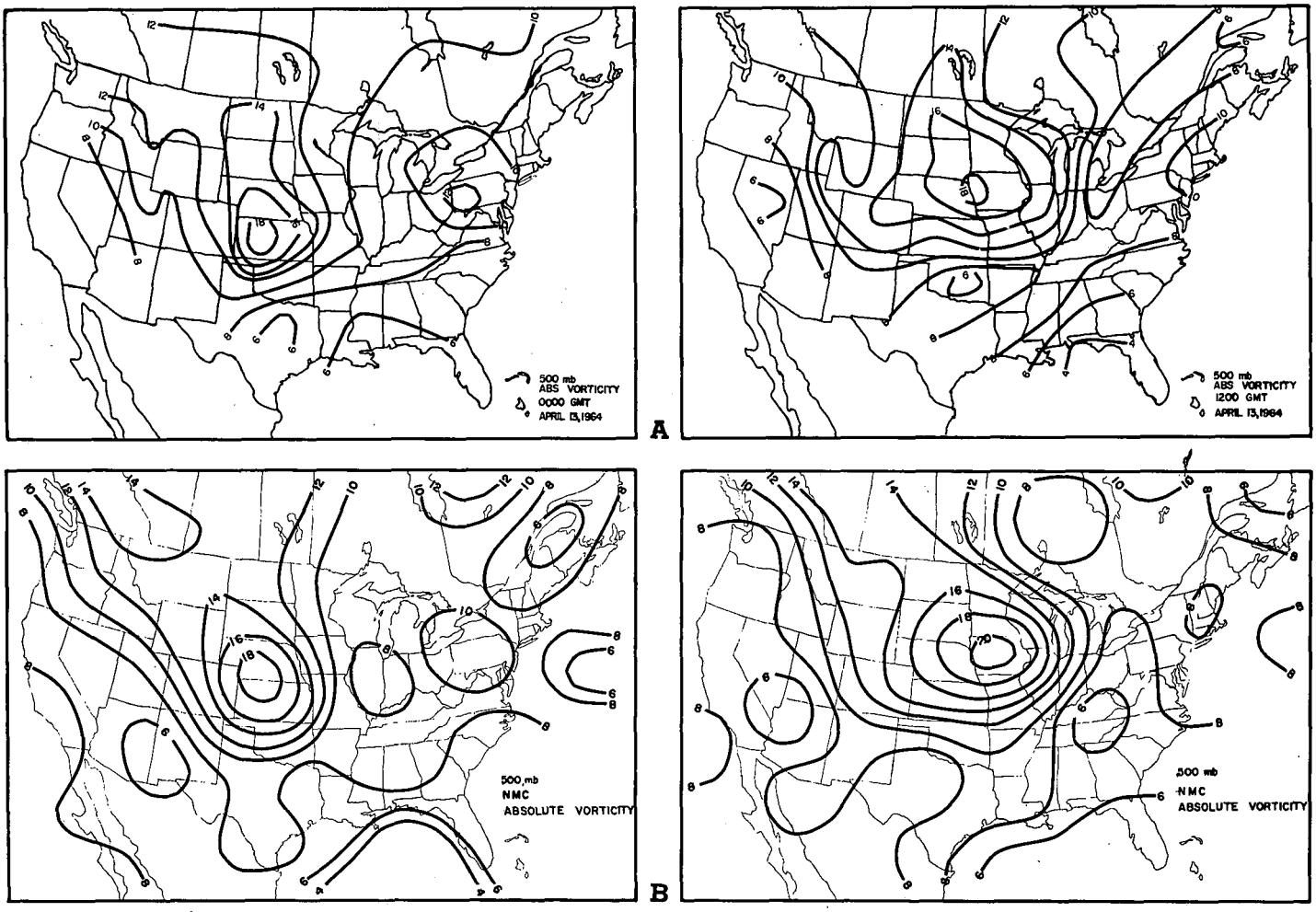

FIGURE 6.—The 500-mb absolute vorticity ($10^{-5}s^{-1}$) computed (A) in this study and (B) by NMC.

convergence (—) values in 10^{-5} s^{-1}. At 0000 GMT, low-level convergence is primarily located ahead of the surface frontal positions as expected. Low-level convergence extending behind the surface front reflects the tendency for surface troughs to be displaced westward with height. The maximum convergence of -2×10^{-5} s^{-1} in Nebraska can be associated with the corresponding surface Low center in western Iowa. The major divergence region is located near the western Kansas and Colorado border associated with the surface ridge. At 300 mb on 0000 GMT, divergence occupies much of the region ahead of the 300-mb trough with convergence occurring behind the trough. Of course, at this level of strong wind flow, the divergence field is quite sensitive to cross-isotach flow and to diffluence and confluence patterns, and many of the divergence patterns might be explained with a close analysis of these features. No such general analysis has been attempted here. However, it is of interest to examine the divergence maximum centered over the Texas panhandle. This region is largely nondiffluent but exhibits a particularly strong isotach gradient with flow nearly perpendicular to the isotachs. One might expect strong divergence under such conditions as indicated in figure 5.

At 1200 GMT, the low-level convergence area has moved to the Minnesota-Canada border, consistent with the low-pressure center movement at the surface. This strong convergence center is located north of the divergence center over Kansas, Nebraska, and Missouri, as expected with an occluded cyclone of the type shown here. The remaining convergence areas reflect essentially the same features noted at 0000 GMT. At 300 mb, a divergence maximum is located ahead of the trough, but once again it is apparent that a complete description of the upper level divergence field might be best accomplished by a detailed analysis of cross-isotach and diffluent flow regions.

Vertical Motions

Figure 4 shows the 500-mb vertical motions computed in this study (dashed lines). Contour lines at 500-mb (solid lines) are superimposed, and upward motion regions are shaded. At 0000 GMT, the primary region of upward motion is located ahead of the major trough with the primary maxima of -7 μbar/s over northern Missouri and the Texas panhandle. The Missouri maximum is located downwind of the maximum vorticity center and is no doubt an important factor in the subsequent development of the surface cyclone. Secondary maxima over New York State and the central Rocky Mountains show good correlation with minor troughs west of those regions. The distribution of precipitation generally reflects the influence of midtropospheric vertical motions and low-level convergence (fig. 3). The Panhandle upward motion maxi-

mum is of special interest, because, despite its magnitude, it shows no correlation with precipitation nor was any cloud indicated in the corresponding NMC surface chart. Examination of low-level and high-level divergence fields indicates that this strong center of upward motion is induced by the previously discussed strong divergence at 300 mb; and, further, since it occurs in the dry air behind the surface front, little moisture is available for production of clouds. It is also interesting to note that this maximum occurs just east of the location of a new surface Low that appeared later at 1200 GMT

At 1200 GMT, the general vertical motion field once again reflects the 500-mb wave features. The vertical motion maximum associated with the surface and 500-mb Low decreases from -7 to -3 μbar/s, although the wave has obviously deepened. The following partial explanation of this apparent inconsistency is offered. Recall, from the discussion of the vorticity estimates, that the vorticity of the system at 500 mb had increased, as would be expected, but that the maximum has remained constant, the latter being accomplished by an exchange between the curvature and shear components of the vorticity. The net effect of these two features in this case would be to produce a general decrease in the vorticity gradient. Further, close comparison of the vorticity fields and 500-mb contour analyses reveals that the flow tends to be more parallel to the vorticity lines at 1200 GMT. This set of circumstances would lead to a reduction in the advection of vorticity from 0000 to 1200 GMT. Further support of these vertical motion estimates is seen in the precipitation analyses, which show a decrease in maximum 6-hr amounts from 0.6 to nearly 0.4 in.

The largest vertical motion maximum at 1200 GMT occurs over the gulf States. This area of strong upward motion is associated with a corresponding large precipitation maximum. This is particularly significant since this precipitation is primarily convective. The current method of computing ω is apparently capable of capturing convective precipitation when the latter is closely linked to a larger scale circulation feature. Another upward maximum center is located over the Texas panhandle associated with the minor low-pressure center that has developed there. Major subsidence is located over Iowa, Missouri, Oklahoma, and Nebraska as expected from the high-pressure ridge penetrating this region. Also, subsidence occurs from the central Great Lakes eastward through southern Canada. The eastern portion of this region lies east of a prominent 500-mb ridge. The remaining portion is apparently dominated by convergence at 300 mb, which is suggested by the strong cross-isotach flow in this region (fig. 5B). The areas of greater than 6/8 cloud cover are depicted in figure 3 by scalloped lines. These also show good correlation with the 500-mb vertical motions.

Finally, an analysis of 500-mb vorticity and adjusted vertical motions determined from the linear Taylor's series mentioned earlier (not shown) revealed patterns over the central United States similar to those presented here. However, the isopleths exhibited numerous spurious and irregular smaller scale centers and undulations, suggesting the presence of computational noise in the results. In addition, the linear model calculations did not reproduce the large upward motion center associated with the convective precipitation region in the southeastern United States at 1200 GMT.

4. CONCLUDING REMARKS

The use of radiosonde wind data, which are known to possess errors, to compute a sensitive parameter such as horizontal divergence is undoubtedly a subject of some controversy. It seems to the authors, however, that the use of alternate representations of the wind field, required to produce stable numerical predictions, must necessarily risk smoothing of synoptic scale features that may be of critical importance in diagnostic studies. The results of this study indicate that the use of raw wind data in a computational model that retains quadratic variations in the wind field and incorporates a physically realistic adjustment technique offers some hope of effectively reducing divergence and vertical motion errors while retaining major and, to some extent, subtle temporal and spatial variations evident in migrating synoptic scale systems.

APPENDIX: INTERPOLATION OF MISSING WIND DATA

A problem noted by Smith (1971) when utilizing radiosonde data for kinematic computations is that observations may sometimes be missing, especially at higher atmospheric levels. If wind data at less than five consecutive levels at a station were missing but observed data were available at the next higher level, the missing winds were estimated by linear interpolation in the vertical. Otherwise, missing winds at a station were generated by a weighted linear interpolation utilizing available data at the same level from surrounding stations.

A study of missing wind data shows that in most cases the reason for data absence is the occurrence of strong winds. To use surrounding data in an interpolation scheme and still produce an estimate that reflects the presence of a wind maximum, one must give added weight to those surrounding data points recording relatively stronger wind speeds. To accomplish this, we multiplied the observed wind speeds at surrounding stations by a weighting value WE_i, where i stands for the ith surrounding station. This value is determined by comparing u_i with the surrounding station value having the smallest wind speed, u_k. Empirical testing indicated that a function of the form

$$WE_i=\left(\frac{u_i}{u_k}\right)^{1/2} \tag{9}$$

was suitable in most cases. However, when u_k was unusually small (e.g., less than 20 m/s at 300 mb), eq (9) tended to provide too heavy a weighting. Therefore, for

cases in which $(u_i/u_k) \geq 3$, the weighting value, was computed as

$$WE_i = \left(\frac{u_i}{u_k}\right)^{1/3}. \quad (10)$$

Finally, if less than four surrounding stations had available data or if data were missing at all levels, WE_i was set equal to one. The net effect of these procedures was to provide weighting values that never exceeded the value two. After multiplying u_i by its corresponding WE_i, we interpolated the wind speed at the interior station (u_0) linearly by the inverse of its distance, d_i, from surrounding stations by the equation

$$u_0 = \frac{\sum_{i=1}^{N} \left(WE_i \frac{u_i}{d_i}\right)}{\sum_{i=1}^{N} \frac{1}{d_i}}. \quad (11)$$

Wind directions were interpolated setting WE_i equal to one.

Figure 5 shows the 300-mb streamline and isotach analysis for 0000 and 1200 GMT on Apr. 13, 1964. Also plotted on the maps are points with interpolated wind speeds and directions. Although observed values are not plotted, the continuity of the isotach-streamline analyses shows clearly that the interpolated values are well within the limits of expected values at these points. Similar analyses setting WE_i equal to one for all wind speeds tended to show deviations from continuity at interpolated points.

ACKNOWLEDGMENTS

The authors are indebted to Dayton Vincent and Ernest Agee of Purdue University, to Ernest Kung of the University of Missouri, and to T. N. Krishnamurti of Florida State University, for their helpful suggestions and encouragement. Special thanks also goes to Kenneth Dowell and Thomas Adang for their assistance in computer programming, data plotting, and figure drafting, and to Sue Gray and Judi Prangley for typing the manuscript. This research was supported by the National Science Foundation under grants GA 10933 and GA 10933 #1.

REFERENCES

Bellamy, John Carey, "Objective Calculations of Divergence, Vertical Velocity and Vorticity," *Bulletin of the American Meteorological Society*, Vol. 30, No. 2, Feb. **1949**, pp. 45–49.

Cressman, George P., "A Three-Level Model Suitable for Daily Numerical Forecasting," National Meteorological Center *Technical Memorandum* No. 22, U.S. Department of Commerce, Weather Bureau, Washington, D.C., **1963**, 22 pp.

Danielsen, Edwin F., "Research in Four-Dimensional Diagnosis of Cyclonic Storm Cloud Systems," *Scientific Report* No. 1, Contract No. AF19 (628)–4762, Department of Meteorology, Pennsylvania State University, University Park, Jan. **1966**, 53 pp.

Duvedal, T., "Upper-level Wind Computation With Due Regard to Both the Refraction of Electromagnetic Rays and the Curvature of the Earth," *Geophysica*, Vol. 8, No. 2, Helsinki, Finland, **1962**, pp. 115–124.

Ellsaesser, Hugh W., "JNWP Operational Models," Joint Numerical Weather Prediction Office *Note* No. 15, revised edition, U.S. Department of Commerce, Weather Bureau, Washington, D.C., Oct. **1960**, 33 pp.

Endlich, R. M., and Clark, J. R., "Objective Computation of Some Meteorological Quantities," *Journal of Applied Meteorology*, Vol. 2, No. 1, Feb. **1963**, pp. 66–81.

Fankhauser, James C., "Convective Processes Resolved by a Mesoscale Rawinsonde Network," *Journal of Applied Meteorology*, Vol. 8, No. 5, Oct. **1969**, pp. 778–798.

Graham, Roderick D., "A New Method of Computing Vorticity and Divergence," *Bulletin of the American Meteorological Society*, Vol. 34, No. 2, Feb. **1953**, pp. 68–74.

Haltiner, George J., and Martin, Frank L., *Dynamical and Physical Meteorology*, McGraw-Hill Book Co., Inc., New York, N.Y., **1957**, 470 pp.

Kreitzberg, Carl W., "The Mesoscale Wind Field in an Occlusion," *Journal of Applied Meteorology*, Vol. 7, No. 1, Feb. **1968**, pp. 53–67.

Krishnamurti, T. N., "A Diagnostic Balance Model for Studies of Weather Systems of Low and High Latitudes, Rossby Number Less Than 1," *Monthly Weather Review*, Vol. 96, No. 4, Apr. **1968***a*, pp. 197–207.

Krishnamurti, T. N., "A Study of a Developing Wave Cyclone," *Monthly Weather Review*, Vol. 96, No. 4, Apr. **1968***b*, pp. 208–217.

Kung, Ernest C., "A Scheme for Kinematic Estimate of Large-Scale Vertical Motion With an Upper-Air Network," *Quarterly Journal of the Royal Meteorological Society*, Vol. 98, No. 416, London, England, Apr. **1972**, pp. 402–411.

Landers, Holbrook, "A Three-Dimensional Study of the Horizontal Velocity Divergence," *Journal of Meteorology*, Vol. 12, No. 5, Oct. **1955**, pp. 415–427.

Lateef, M. A., "Vertical Motion, Divergence, and Vorticity in the Troposphere Over the Caribbean, August 3–5, 1963," *Monthly Weather Review*, Vol. 95, No. 11, Nov. **1967**, pp. 778–790.

Miller, Albert, and Panofsky, Hans Arnold, "Large-Scale Vertical Motions and Weather in January, 1953," *Bulletin of the American Meteorological Society*, Vol. 39, No. 1, Jan. **1958**, pp. 8–13.

O'Brien, James J., "Alternative Solutions to the Classical Vertical Velocity Problem," *Journal of Applied Meteorology*, Vol. 9, No. 2, Apr. **1970**, pp. 197–203.

O'Neill, Thomas H. R., "Vertical Motion and Precipitation Computations," *Journal of Applied Meteorology*, Vol. 5, No. 5, Oct. **1966**, pp. 595–605.

Panofsky, Hans Arnold, "Large-Scale Vertical Velocity and Divergence," *Compendium of Meteorology*, American Meteorological Society, Boston, Mass., **1951**, 1334 pp. (See pp. 639–646.)

Schmidt, Phillip J., and Johnson, Donald R., "Use of Approximating Polynomials to Estimate Profiles of Wind, Divergence, and Vertical Motion," *Monthly Weather Review*, Vol. 100, No. 5, May **1972**, pp. 345–353.

Smith, Phillip J., "An Analysis of Kinematic Vertical Motions," *Monthly Weather Review*, Vol. 99, No. 10, Oct. **1971**, pp. 715–724.

Thompson, Philip Duncan, *Numerical Weather Analysis and Prediction*, Macmillan Co., New York, N.Y., **1961**, 170 pp.

[*Received February 25, 1972; revised October 4, 1972*]

UDC 551.524.77:551.576.1:551.507.362.2:551.506.7(084.1)(76+77)

PICTURE OF THE MONTH
VHRR Imagery of an Inversion

L. F. HUBERT and RUSSELL KOFFLER—*National Environmental Satellite Service, NOAA, Suitland, Md.*

Figures 1A and 1B are simultaneous views in the visible and in the infrared, respectively, of an area extending from the southern tip of Lake Michigan to the Gulf of Mexico. Taken from the very high resolution radiometers (VHRR) aboard the polar orbiting satellite NOAA 2, these two channels (from 0.4 to 0.6 μm and 10.5 to 12.5 μm) provide resolution of 1 km at the satellite subpoint.

Infrared radiance measurements are converted to pictures in such a way that the warm surfaces (greater radiance) are darker than cold surfaces (lesser radiance). Hence, cold clouds are depicted as lighter than their warm, dark background, so cloud pictures appear to be similar to those made with visible light. Differences do exist, however, providing information that is not available from a single channel. This picture pair is a good example.

These views show the existence of two strata of clouds—one at the base and the other near the top of a strong inversion. In this situation, the higher clouds are considerably warmer than the lower layer; therefore, they appear as dark areas on the infrared picture. Lettered features indicate where this inversion effect is revealed.

Region a is an elongated patch of thin clouds so tenuous as to be almost undetectable on figure 1A—the underlying cloud pattern is clearly visible through the elongated patch. Only a few bright streaks of dense lines and their shadows on the underlying cloud deck show that the elongated patch is indeed the higher layer. In the infrared view, however, the patch appears as a dark area indicating that it is warmer. Equally important, comparison of the pictures shows that the patch is nearly transparent to

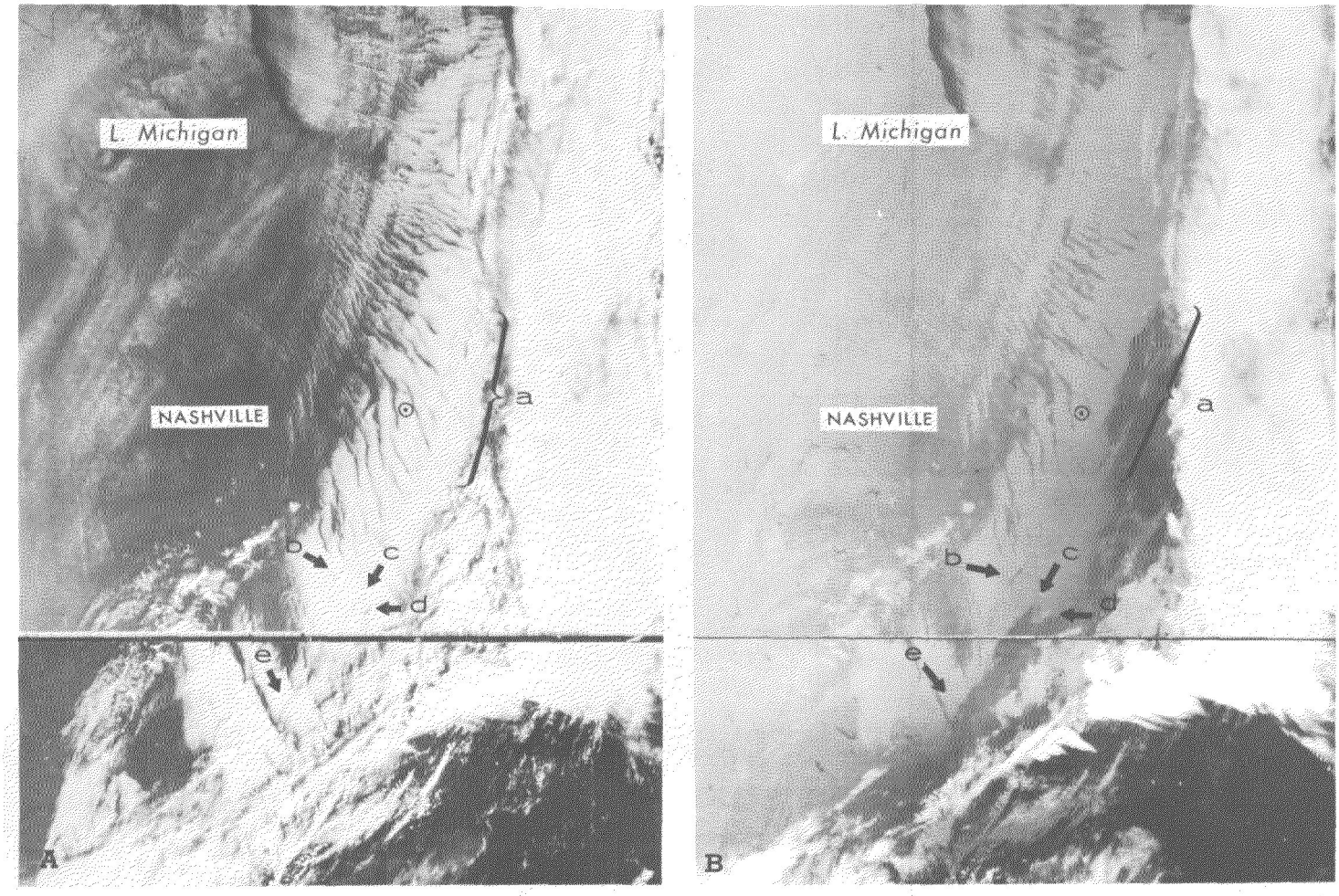

FIGURE 1.—(A) a visible picture and (B) a picture sensed in the water vapor window, both made with the NOAA 2 very high resolution radiometer at 1500 GMT, Dec. 6, 1972.

visible radiation but nearly opaque to infrared radiation. The infrared view also pictures a cold cloud line running along the axis of the warm patch, apparently at the same elevation as the small feature, discussed later, at d.

Other warm clouds extend to the southwest. On Figure 1A, b and c indicate bright streaks bounded by shadows on their northwest side, and e indicates the edge of a patch similar to the one at a. The small cloud line at d is colder than its neighbors. In the visible picture it is bright and casts a wider shadow than the feature at c, but on figure 1B it shows up as a cold (bright) cloud band, colder even than the underlying cloud deck.

Figure 2, the sounding taken at Nashville, Tenn., within 3 hr of the picture time, confirms our interpretation and enables us to estimate cloud heights. Cloud patches from e to a lie in the warmest air, perhaps somewhere in the layer 850–915 mb, while the underlying cloud deck is topped near 950 mb. Cloud top of the band at d, however, is colder than the lowest cloud layer and therefore must lie above 750 mb. The sounding suggests that the pressure might be 620–630 mb.

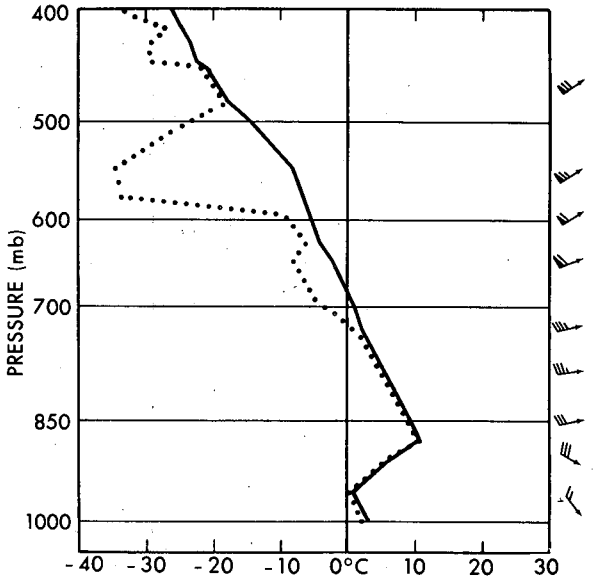

FIGURE 2.—Rawinsonde sounding from Nashville, Tenn., at 1200 GMT, Dec. 6, 1972.